Receptor-interacting protein kinase-1 ablation in liver parenchymal cells promotes liver fibrosis in murine NASH without affecting other symptoms

Muhammad Farooq, Melanie Simoes Eugenio, Claire Piquet-Pellorce, Sarah Dion, Celine Raguenes-Nicol, Kathleen Santamaria, Ghania Hounana Kara-Ali, Thibaut Larcher, Marie-Therese Dimanche-Boitrel, Michel Samson, et al.

Receptor interacting protein kinase-1 ablation in liver parenchymal cells promotes liver fibrosis in murine NASH without affecting other symptoms

Muhammad Farooq[1,2#], Mélanie Simoes Eugénio[1#], Claire Piquet-Pellorce[1], Sarah Dion[1], Céline Raguenes-Nicol[1], Kathleen Santamaria[1], Ghania Hounana Kara-Ali[1], Thibaut Larcher[3], Marie-Thérèse Dimanche-Boitrel[1], Michel Samson[1*¶] and Jacques Le Seyec[1*]

[1] Univ Rennes, Inserm, EHESP, Irset (Institut de recherche en santé, environnement et travail) - UMR_S 1085, F-35000 Rennes, France.

[2] Department of Clinical Sciences, College of Veterinary and Animal Sciences, University of Veterinary and Animal Sciences, Jhang, Lahore, Pakistan.

[3] INRAE, Oniris, UMR0703, APEX, Nantes, France

[#] or *Authors with similar signs contributed equally.

[¶] **Corresponding author**: Michel Samson, INSERM U1085, Irset, Université de Rennes 1, 2 av Prof Leon Bernard, 35043 Rennes cedex, France ; Tel: (+33) (0)2 23 23 69 11 ; Fax : (+33) (0)2 23 23 50 55 ; michel.samson@univ-rennes1.fr

Electronic word count: 3078

Number of figures and tables: 5 figures

Acknowledgments

We are grateful to Pr. M. Bertrand and Pr. P. Vandenabeele, both from the Inflammation Research Center, VIB (Belgium) for the provision of Ripk1^{LPC-KO} mice. We would like to thanks the "Laboratoire de Biochimie-Toxicologie" from the "CHU de Rennes" for transaminase measurements. For immunohistochemistry analysis, bead-based immunoassays, flow cytometry analysis and animal house facilities, we would like to acknowledge the dedicated platforms (i.e. H2P2, flow cytometry and cell sorting, and animal house platforms) of SFR Biosit – UMS 3480, US_S 018, France.

Abstract

Non-alcoholic steatohepatitis (NASH), a chronic liver disease that emerged in industrialized countries, can further progress into liver fibrosis, cirrhosis and hepatocellular carcinoma. In the next decade, NASH is predicted to become the leading cause of liver transplantation, the only current interventional therapeutic option. Hepatocyte death, triggered by different death ligands, plays key role in its progression. Previously, we showed that the receptor interacting protein kinase-1 (RIPK1) in hepatocytes exhibits a protective role in ligand-induced death. Now, to decipher the role of RIPK1 in NASH, *Ripk1*$^{LPC\text{-}KO}$ mice, deficient for RIPK1 only in liver parenchymal cells, and their wild-type littermates (*Ripk1*$^{fl/fl}$) were fed for 3, 5 or 12 weeks with high-fat high-cholesterol diet (HFHCD). The main clinical signs of NASH were analysed to compare the pathophysiological state established in mice. Most of the symptoms evolved similarly whatever the genotype, whether it was the increase in liver to body weight ratio, the steatosis grade or the worsening of liver damage revealed by serum transaminase levels. In parallel, inflammation markers followed the same kinetics with significant equivalent inductions of cytokines and a main peak of hepatic infiltration of immune cells at 3 weeks of HFHCD. Despite this identical inflammatory response, more hepatic fibrosis was significantly evidenced at week 12 in *Ripk1*$^{LPC\text{-}KO}$ mice. This coincided with over-induced rates of transcripts of genes implied in fibrosis development (*Tgfb1*, *Tgfbi, Timp1* and *Timp2*) in *Ripk1*$^{LPC\text{-}KO}$ animals. In conclusion, our results show that RIPK1 in hepatocyte limits the progression of liver fibrosis during NASH.

Electronic word count: 243

Keywords

NASH; RIPK1; Fibrosis; Hepatocyte

Introduction

The evolution to a sedentary lifestyle, also accompanied by more caloric diet intakes, is responsible for the emergence of a new silent epidemic in human. Indeed, non-alcoholic fatty liver diseases (NAFLD) would nearly affect a quarter of the world's population, with some geographical disparity [1, 2]. These diseases cover a spectrum of hepatic disorders ranging from benign steatosis to inflammatory status, defined as non-alcoholic steatohepatitis (NASH), responsible for the development of fibrosis that will eventually worsen, leading to cirrhosis and even hepatocellular carcinoma (HCC) with high rates of morbidity and mortality[3]. NASH is currently the second leading cause of liver transplantation in USA after hepatitis C and is expected to predominate in the future among the US and European population [4].

Although influenced by genetic and epigenetic factors, the pathogenesis of NAFLD would result from multiple concomitant insults originating from gut and adipose tissue. Thus, a "multiple parallel hits" theory has recently been proposed to explain the NAFLD pathogenesis leading to NASH [5, 6]. At this pathological stage, an inflammatory state is established due to the stress experienced by hepatocytes. In parallel, hepatocyte death is compensated by the activation of a regeneration process. Repetition of these events over time eventually leads to liver tissue remodeling, characterized by the development of fibrosis. Activated Kupffer cells (KCs), infiltrating macrophages and damaged hepatocytes release various cytokines that activate quiescent hepatic stellate cells (HSCs) in collagen-secreting myofibroblasts [7]. The hepatic fibrosis results from an imbalance characterized by an overproduction of extracellular matrix (ECM) [8] and an exacerbated inhibition of the HSCs and KCs secreted matrix metalloproteinases (MMPs) by different specific endogenous tissue inhibitors of metalloproteinases (TIMPs) [9, 10].

Hepatocyte death fuels the inflammation that causes liver fibrosis and eventually promotes HCC development when chronic [11, 12]. The death factors, tumor necrosis factor (TNF), Fas Ligand (FAS-L) and TNF-related apoptosis-inducing ligand (TRAIL), are found overexpressed in liver tissue during NASH [7]. Cellular responses induced by these members of the TNF superfamily involve the receptor interacting protein kinase-1 (RIPK1) [13-15]. Within the intracellular transduction pathway specifically triggered by TNF, RIPK1 directs signaling to a pathway of cell survival or death, either by caspase-dependent apoptosis or by necroptosis regulated by RIPK3 and the mixed lineage kinase domain-like protein (MLKL). The role of this molecular switch between cell survival and death has been widely investigated during acute hepatitis. Thus, in murine models of viral [16] or immune-mediated hepatitis [17], RIPK1 expressed in hepatocytes promotes their survival in a microenvironment rich in death ligands. During NASH, the associated dysfunction of the intestinal barrier leads to significant leaks of pro-inflammatory bacterial pathogen associated molecular patterns (PAMPs) to which the liver is exposed [18-21]. Thus, it has been demonstrated that RIPK1 expressed in hepatocytes protects them from TNF-dependent death in an inflammatory context induced by PAMPs [22-24]. Recently, the role of RIPK1 in NAFLD started to generate interest. Indeed, patients suffering from NAFLD exhibit increased hepatic *Ripk1* transcripts

and plasma RIPK1 levels [25, 26]. Besides, mice with diet-induced NASH developed less liver injury, inflammation and fibrosis when treated with a pharmacological RIPK1 inhibitor [25] or when mice display a constitutive knock-in mutation responsible for RIPK1 kinase activity deficiency [26]. While RIPK1 kinase activity in macrophages seemed to appear central in the development of NASH syndromes [26], within hepatocytes, it would control the hepatocyte steatosis grade [25]. This highlights the possible key role of RIPK1 present specifically in hepatocytes in high fatty acid induced liver injury. In this context, we investigated the functions of RIPK1 in liver parenchymal cells during high-fat high-cholesterol diet (HFHCD) induced NASH, mimicking human disease [27].

Methods

Animals

Male C57BL/6J mice, with *Ripk1*$^{LPC\text{-}KO}$ (deficient for RIPK1 specifically in liver parenchymal cells) or *Ripk1*$^{fl/fl}$ (control littermates with homozygous floxed *Ripk1* gene) genotypes [17] were fed either a standard diet (SD; # 2016, Teklad Global 16% Protein Rodent Diet, Envigo, Madison, WI) or a high-fat high-cholesterol diet enriched in cholate (HFHCD, #9G21, LabDiet, St. Louis, MO) *ad libitum* for 3, 5 or 12 weeks. Mice were euthanized in the morning without prior fasting. Genotyping was performed by conventional PCR for *Alfp-Cre* gene from tail-extracted DNA. The specific deficiency of *Ripk1*in the hepatocytes of *Ripk1*$^{LPC\text{-}KO}$ mice has already been checked [22]. Experiments included homogeneous groups of age-matched male mice.

Histological and biochemical analysis

The histopathological study of livers was performed on hematoxylin and eosin (H&E)-stained tissue sections to characterize steatosis, lobular infiltrates and hepatocyte ballooning. Oil-Red O (ORO) staining with a hematoxylin counterstaining was applied on frozen sections of liver specimens to specifically visualize intracellular lipid droplets. The proportion of ORO-labeled surface was determined using the HALO software (Indica Labs, Albuquerque, NM). Fibrosis was assessed after Sirius red coloration by evaluating the proportion of the stained area, using the NIS-Elements software (Nikon). Plasma alanine transaminases (ALT) were measured according to the International Federation of Clinical Chemistry and Laboratory Medicine (IFCC) primary reference procedures using Olympus AU2700 Auto-analyser® (Olympus Optical, Tokyo, Japan). High-resolution images were used to study H&E-stained sections. The same senior veterinary pathologist blindly scored all livers for NAFLD activity lesions (NAS). A previously described histological scoring system was used to describe main features of NASH [28, 29]. Briefly, 3 histological variables commonly described in NASH were individually assessed: (i) macrovesicular steatosis was graded (0–3) based on percent of hepatocytes involved (0 is none; 1 is up to 33%; 2 is 33 to 66%; 3 is more than 66%); (ii) Hepatocellular ballooning and disarray and (iii) lobullar inflammation were graded as none, mild, moderate, and severe (0–3).

RNA Isolation and RT-qPCR

Total RNA was extracted from mice liver tissues using the NucleoSpin® RNA kit (Macherey-Nagel, #740955). First-strand cDNA was synthesized using the High-Capacity cDNA Reverse Transcription Kit (Applied Biosystems, #4368813, Foster City, CA, USA). Real-time quantitative PCR was performed using the double-strand specific SYBR® Green system (Applied Biosystems, #4367659) on CFX384 Touch™ Real-Time PCR Detection System (Biorad). Each measurement was performed in triplicate. The relative gene expression was normalized against the *18S* gene expression. Samples from SD-fed mice were used as reference for mRNA expression (control mRNA level was arbitrarily set at 1). The primer sequences are all depicted in Table S1 in supporting information.

Serum cytokine immunoassay by flow cytometry

Murine cytokines (IL1α, IL1β, IL6, IL10, IL12p70, IL17A, IL23, IL27, CCL2, IFNβ, IFNγ, TNF, and GM-CSF) were quantified by bead-based immunoassays according to manufacturer protocol, using a filter plate and a vacuum filtration system for washing steps (BioLegend's LEGENDplex™ Mouse Inflammation Panel, multi-analyte flow assay kit). Samples were analyzed on a LSR X-20 Fortessa™ flow cytometer (BD Biosciences). Data not shown in the main figures are depicted in Fig. 1S. For the dosage of some cytokines, values corresponding to sensitivity threshold were used for statistical analysis of potential regulations for samples with cytokine concentrations below the specific sensitivity threshold.

Isolation of liver immune cells and flow cytometry

Immune cells were isolated from livers as previously described [30]·[31]. Before liver excision, the organ was flushed by perfusion of PBS through *inferior vena cava*, to remove non-infiltrated blood cells. Isolated livers were then ground on a 70-µm cell strainer. Parenchymal cells were removed by decantation for 1h. Cells in suspension were recovered by centrifugation and then resuspended in 35% isotonic Percoll (GE Healthcare Life Science) for a new centrifugation, before red blood cell lysis. Cells were resuspended in staining buffer (10% fetal calf serum in PBS) and incubated with LIVE/DEAD fixable green stain (Thermo Fisher Scientific, #L34959) to exclude dead cells. Cells were also labeled with an anti-CD16/32 antibody (clone 2.4G, BD Pharmingen) to block non-specific binding. Cells were then labeled with the appropriate fluorochrome-conjugated antibodies/reagents (Table S2) according to the manufacturer's instructions. Stained cells were analyzed on a LSR X-20 Fortessa™ flow cytometer (BD Bioscience) and the data analyzed using Flowlogic™ (MACS Miltenyi Biotec). Doublets and dead cells were excluded on the basis of forward/side scatter and LIVE/DEAD labeling, respectively. The immuno-phenotyping used was made on the appropriate size-FSC (forward side scatter)/structure-SSC (side scatter) gates and was as follows: B-lymphocytes: CD19+/CD3- cells; T-lymphocytes: CD3+/TCRVβ+/NK1.1-/CD19- on which CD4+ and CD8+ were distinguished and Tregs as FoxP3+ within the TCD4+

population; NKT cells: CD3+/NK1.1+/CD19-; NK cells: CD3-/NK1.1+/CD19-; within the myeloid CD19-/CD3-/NK1.1-/CD11b+ cell population, neutrophils were selected as GR1high and macrophages as GR1int (Fig. 2S). We calculated the percentage of each immune cell population, by considering the sum of events of all immune cell populations analyzed (sum of T, NK, NKT, B cells and myeloid cells) as 100% of the total immune cells. The absolute number in each immune cell population was calculated by multiplying the percentage of each population by the total number of immune cells.

Statistical analysis

The results are expressed as the means ± SEM for each group of mice. Mean differences between experimental groups were assessed using the nonparametric Mann-Whitney U-test, as implemented in GraphPad Prism5 software. Significance is shown as follows: * $p < 0.05$, ** $p < 0.01$ and *** $p < 0.001$.

Results

HFHCD promoted overexpression of hepatic transcripts of death ligands, their cognate receptors and of RIPK1.

Hepatocyte death occurring during NASH fuels the inflammatory status of the liver. These events are thought to be partly affected by an imbalance within cell death signalling pathways. Thus, to evaluate these types of disruption in HFHCD-fed mice, transcript rates of death ligands and their receptors were compared to those issued from livers of age and sex matched mice fed with SD. Twelve weeks of HFHCD resulted in upregulation of all tested transcripts of death ligands (TNF, FAS-L and TRAIL) as well as of their cognate receptors (TNFR1, TNFR2, FAS and DR5) (Fig. 1). Downstream of these cues, the RIPK1 protein redirect the intracellular signal towards inflammatory or cell death processes. By analysing the RIPK1 transcript, it turned out that higher concentrations were also detected in the liver of mice fed during 12 weeks of HFHCD (Fig. 1).

Severity of HFHCD-induced hepatomegaly and liver damage was not affected by *Ripk1*-depletion in liver parenchymal cells.

HFHCD disturbed the transcript level of RIPK1 in the liver, a key death signal switch, but to know whether this kinase influences the NASH physiopathology, mice deficient for *Ripk1* specifically in liver parenchymal cells ($Ripk1^{LPC\text{-}KO}$) and their wild type littermates ($Ripk1^{fl/fl}$) were subjected to this diet during 3, 5 or 12 weeks. First, body weight monitoring revealed no statistically significant change between both genotypes (Fig. 2A, left panel). The average daily food consumption per animal was limited to 1.6 g, while it reached 3.5 g with the SD. However, the daily calorie intake remained similar, around 10.5 kcal. In contrast, a progressive hepatomegaly systematically settled in all animals whatever the genotype (Fig 2A, right panel). Along with this symptom, hepatic tissue degradation progressively worsened over

time as evidenced by plasma levels of transaminases (Fig. 2B). Concomitantly, a similar steatosis settled in all animals, irrespective of the genotype (Fig. 2C and 2D).

***Ripk1* defect in parenchymal liver cells did not reshape hepatic inflammatory response during NASH.**

Systematic histological analysis of H&E-stained liver sections showed the appearance of hepatocyte ballooning and of local accumulation of immune cells as early as 3 weeks post-HFHCD feeding (Fig. 2D). Thus, the evaluation of the NAS score showed a progressive worsening of the hepatic histology over time, without detecting any difference between the two genotypes (Fig. 2E). To quantitatively compare the hepatic inflammatory status induced by the HFHCD feeding in *Ripk1*$^{fl/fl}$ and *Ripk1*$^{LPC\text{-}KO}$ mice, the expression alteration of major pro-inflammatory cytokines was assessed. Whether at hepatic transcript levels or at plasma protein levels, significant progressive increases occurred for TNF, IL6 and CCL2 as the HFHCD intake continued for 12 weeks. Although some significant differences appeared between the two genotypes at the mRNA level, the serum protein levels of these cytokines never differed between genotypes regardless of diet time (Fig. 3). Otherwise, for IFNβ and IL27, only a transient protein overexpression arose in blood samples taken at 3 weeks of HFHCD regardless of genotype, a timing that coincided with immune cell infiltration wave in the liver (see below). Investigations on other death factors such as FASL, TRAIL and their cognate receptors have been conducted at mRNA levels. All gradually increased as the diet continued for up to 12 weeks, without any detectable differences between both genotypes (Fig. 3S). The hepatic inflammation was further characterized by isolating the immune cells from *Ripk1*$^{fl/fl}$ and *Ripk1*$^{LPC\text{-}KO}$ mouse livers that have been on SD or HFHCD for 3, 5 or 12 weeks. A flow cytometry approach was applied to identify and enumerate cell types. Irrespective of the genotype, huge recruitment of inflammatory cells appeared in liver at 3 weeks post-HFHCD feeding, which then decreased at 5 and 12 weeks post-HFHCD feeding (Fig. 4, upper panel). We then distinguished the significant changes in liver immune cell populations among lymphoid (LT4, LT8, LTregs, NK, NKT and LB) and myeloid (macrophages and neutrophils) cells during the course of NASH development. All intrahepatic immune cells were significantly more numerous at 3 weeks of HFHCD, with different induction rates for each cell type. Thus, macrophages and lymphocytes were more than 10 times more abundant, while the number of NKT cells only doubled. Over longer periods of HFHCD, this excess of infiltrating immune cells progressively diminished, with maintenance of a still large number of macrophages and LT8 at the 5th week. Compared to a healthy liver, most immune cells remained slightly more abundant in livers after 12 weeks of HFHCD, except neutrophils, NK and NKT cells. Thus, as previously reported [32], the NKT cells were almost depleted at 12 weeks post-HFHCD feeding.

All these tested biological parameters evaluated during the course of the disease never differed according to the genotype of the mice.

RIPK1 partially protected from HFHCD-induced fibrosis.

NASH induced by HFHCD led to the progressive development of liver fibrosis. A Sirius red staining was performed on liver sections of mice subjected to SD or HFHCD. Collagen accumulated in the liver tissue of all animals fed with the HFHCD. This deposit increased over time but reached significantly higher levels at 12 weeks post-HFHCD feeding in *Ripk1*$^{LPC\text{-}KO}$ mice as compared to their *Ripk1*$^{fl/fl}$ littermates (Fig. 5A).

The mRNA levels of several genes involved, directly or indirectly in the remodelling of the ECM were evaluated in the liver of *Ripk1*$^{fl/fl}$ and *Ripk1*$^{LPC\text{-}KO}$ mice during the kinetics of HFHCD (Fig. 5B). A progressive increase over time was found for all studied mRNAs, in both animal groups. Thus, the upregulation of the transforming growth factor beta 1 (*Tgfb1*) transcript followed the gradual worsening of fibrosis. The mRNA of this cytokine, which is a key inducer of the trans-differentiation of HSCs into myofibroblasts that produce the excess of ECM, was overinduced in *Ripk1*$^{LPC\text{-}KO}$ mice at weeks 3 and 12. In parallel, a time-dependant enrichment of collagen type I alpha 1 chain (*Col1a1*) mRNA occurred without quantitative difference between the two tested genotypes. Similarly, mRNA amounts of the transforming growth factor beta-induced (*Tgfbi*) steadily increased, but reached a significant higher level in *Ripk1*$^{LPC\text{-}KO}$ mice after 12 weeks of HFHCD. While a significant over-induction of liver transcripts was observed for two tissue inhibitors of metalloproteinases (*Timp1* and *Timp2*) in the hepatic tissue of *Ripk1*$^{LPC\text{-}KO}$ mice, no significant over-induction was measured for the matrix metalloproteinase-2 (*Mmp-2*) and for the NADPH oxidase 2 (*Nox2*). This last enzyme has been described to participate to the production of reactive oxygen species (ROS) implied in the activation of HSCs [33].

In conclusion, depletion of *Ripk1* in liver parenchymal cells increased liver fibrosis in mice with HFHCD-induced NASH.

Discussion

Cell death plays pivotal role in the progression of NASH [11]. The interaction of various death ligands such as TNF, FAS ligand and TRAIL with their respective cognate receptors TNFR1, FAS and DR5 triggers intracellular signalling resulting in cell death. Transcripts of all these proteins were upregulated in the liver of mice fed with a high fat diet enriched in cholesterol and cholate (HFHCD). These results were consistent with previous studies that showed the involvement of these death ligand-receptor pairs in the pathogenesis of NASH [7, 34, 35]. Thus, while the role of TNF neutralization in the amelioration of liver injury remains controversial, knockout of TRAILR or TNFR1 protects mice from diet-induced NASH [35, 36]. Recently, our team demonstrated the protective role of RIPK1 in TNF, anti-Fas antibody (JO_2) or TRAIL mediated acute liver injury [17, 22, 37]. The scaffolding properties and the kinase activity of RIPK1 respectively control cell survival and cell death [38]. Inhibition of its kinase activity by the Necrostatin-1 (Nec-1) [39] limits both the toxicity of fatty acids on primary mouse hepatocytes [40] and the pathophysiology of NASH induced by methionine choline deficient diet (MCD) [41]. However, this chemical inhibitor shows some drawbacks, its limited specificity and its short half-life [42]. Recently, another RIPK1 inhibitor (RIPA-56) has been shown to limit the main symptoms in mice fed with

a high-fat diet [25]. Further investigations were required to explore the role of RIPK1 in NASH. HFHCD has been shown to reproduce hepatic histological lesions of NASH observed in human liver, including hepatocyte ballooning and injury, inflammation, hepatic insulin resistance and extensive liver fibrosis [27, 32]. Here, we demonstrated that deletion of *Ripk1* specifically in liver parenchymal cells increased liver fibrosis in HFHCD-induced NASH.

The recruitment of inflammatory cells in the liver is a key characteristic in patients with NASH [43]. In an early phase of HFHCD-induced NASH, a massive infiltration of immune cells transiently occurred in mouse livers. These infiltrates contained macrophages, neutrophils, lymphocytes, regulatory T cells, NK and NKT cells. Subsequently, their number tended to decrease while maintaining relative high levels for macrophages and CD8+ T cells, which corresponded to a low-grade inflammatory state in the late phase of NASH. Conversely, NKT cells gradually disappeared as previously described [32, 44-46]. This depletion may be due to their death following their over-activation by macrophages presenting them lipid antigens [46]. *Ripk1* deficiency in liver parenchymal cells never affected the profile of the immune cell population during the course of NASH.

Chemokines and cytokines play also key roles in the development of NASH. In accordance with previous studies, transcripts of *Tnf*, *Il6* and *Ccl2* increased in the liver of *Ripk1*$^{fl/fl}$ control mice fed with HFHCD, as well as plasma levels of the corresponding proteins [43, 45, 47]. While inflammatory cytokine production has been shown to be impaired in *Ripk1* deficient primary or immortalized monocytes [48], its depletion in liver parenchymal cells never affected the HFHCD-induced upregulation of liver transcripts of TNF, IL6 and CCL2 inflammatory cytokines, nor their plasma levels. Similarly, the pattern of inflammatory cells recruited in the liver of *Ripk1*$^{LPC\text{-}KO}$ mice during the progression of HFHCD-induced NASH was not altered.

In response to chronic and persistent liver injury occurring during NASH, the cytokine microenvironment activates HSCs that differentiate into myofibroblasts. This myofibroblastic phenotypic evolution leads to an excessive synthesis of matrix proteins such as collagens, elastin and fibronectins [49, 50]. In parallel, these activated myofibroblast-like HSCs increase their production of proteins involved in the regulation of matrix degradation, including MMPs and their TIMPs. However, a disproportionate activity of TIMPs hampers ECM degradation. Together, these disorders are responsible for the establishment of liver fibrosis [9]. All these pathological imbalances were found in the liver of mice fed with the HFHCD, but *Ripk1* deficiency in liver parenchymal cells significantly increased liver fibrosis. This worsening correlated with a higher significant overexpression of *Tgfb1, Tgfbi, Timp1* and *Timp2* transcripts in *Ripk1*$^{LPC\text{-}KO}$ mice. Although the *Col1a1* and *Mmp2* transcripts increased comparably within both genotypes, fibrosis worsening in the liver of *Ripk1*$^{LPC\text{-}KO}$ mice under HFHCD could result from the differences observed at *Timp1* and *Timp2* transcript levels, since ECM degradation function of MMPs are regulates at the protein levels by TIMPs [51]. Future studies elucidating the role of *Ripk1* in the control of the fibrosis during NASH, will pave the way to unveil the involved mechanism.

Declaration

Funding: This work was supported by the "Contrat de Plan Etat-Région" (CPER) grant named "Infectio"; the "Ligue Contre le Cancer, Comités du Grand Ouest"; the Biology and Health Federative Research Structure of Rennes (Biosit, UMS CNRS 3480 / US INSERM 018) and the "Fondation pour la Recherche Médicale" (FRM # DEQ20180339216). M.F. was supported by a PhD fellowship from the Government of Pakistan (Higher Education Commission). M.S.E. was supported by a PhD fellowship from "Région Bretagne" and "Ministère de l'Enseignement Supérieur et de la Recherche". G.H.K.A. was supported by a PhD fellowship from "Ministère de l'Enseignement Supérieur et de la Recherche".

Conflicts of interest/Competing interests: The authors have no conflicts of interest to declare.

Availability of data and material: All data generated or analysed during this study are included in this published article and its supplementary information files.

Code availability: Not applicable

Authors' contributions: Conceptualization: Muhammad Farooq, Mélanie Simoes Eugénio, Claire Piquet-Pellorce, Sarah Dion, Céline Raguenes-Nicol, Kathleen Santamaria, Ghania Hounana Kara-Ali, Michel Samson and Jacques Le Seyec; Data acquisition: Muhammad Farooq., Mélanie Simoes Eugénio., Claire Piquet-Pellorce, Sarah Dion, Céline Raguenes-Nicol., Kathleen Santamaria, Ghania Hounana Kara-Ali, Michel Samson and Jacques Le Seyec; All authors contributed to data analysis and interpretation. Muhammad Farooq prepared the original draft of the manuscript and generated figures. Michel Samson and Jacques Le Seyec reviewed and edited it.

Ethics approval: Animal studies were reviewed and approved by the "Comité d'Ethique en Expérimentation Animale" (C2EA – 07) under the supervision of the French Ministry of Higher Education and Research (permission #: 5656-2016061401105051). Investigations were carried out in strict compliance with the recommendations in the Guide for the Care and Use of Laboratory Animals, EEC Council Directive 2010/63/EU.

Consent to participate: Not applicable

Consent for publication: Not applicable

References

1. Younossi Z, Anstee QM, Marietti M, Hardy T, Henry L, Eslam M, George J, Bugianesi E (2018) Global burden of NAFLD and NASH: trends, predictions, risk factors and prevention. Nature reviews Gastroenterology & hepatology 15: 11-20. DOI 10.1038/nrgastro.2017.109
2. Younossi ZM, Koenig AB, Abdelatif D, Fazel Y, Henry L, Wymer M (2016) Global epidemiology of nonalcoholic fatty liver disease-Meta-analytic assessment of prevalence, incidence, and outcomes. Hepatology (Baltimore, Md) 64: 73-84. DOI 10.1002/hep.28431
3. Calzadilla Bertot L, Adams LA (2016) The Natural Course of Non-Alcoholic Fatty Liver Disease. International journal of molecular sciences 17. DOI 10.3390/ijms17050774
4. Wong RJ, Aguilar M, Cheung R, Perumpail RB, Harrison SA, Younossi ZM, Ahmed A (2015) Nonalcoholic steatohepatitis is the second leading etiology of liver disease among adults awaiting liver transplantation in the United States. Gastroenterology 148: 547-555. DOI 10.1053/j.gastro.2014.11.039
5. Buzzetti E, Pinzani M, Tsochatzis EA (2016) The multiple-hit pathogenesis of non-alcoholic fatty liver disease (NAFLD). Metabolism: clinical and experimental 65: 1038-1048. DOI 10.1016/j.metabol.2015.12.012
6. Tilg H, Moschen AR (2010) Evolution of inflammation in nonalcoholic fatty liver disease: the multiple parallel hits hypothesis. Hepatology (Baltimore, Md) 52: 1836-1846. DOI 10.1002/hep.24001
7. Hirsova P, Gores GJ (2015) Death Receptor-Mediated Cell Death and Proinflammatory Signaling in Nonalcoholic Steatohepatitis. Cellular and molecular gastroenterology and hepatology 1: 17-27. DOI 10.1016/j.jcmgh.2014.11.005
8. Hemmann S, Graf J, Roderfeld M, Roeb E (2007) Expression of MMPs and TIMPs in liver fibrosis - a systematic review with special emphasis on anti-fibrotic strategies. Journal of hepatology 46: 955-975. DOI 10.1016/j.jhep.2007.02.003
9. Arthur MJ (2000) Fibrogenesis II. Metalloproteinases and their inhibitors in liver fibrosis. American journal of physiology Gastrointestinal and liver physiology 279: G245-249. DOI 10.1152/ajpgi.2000.279.2.G245
10. Jackson BC, Nebert DW, Vasiliou V (2010) Update of human and mouse matrix metalloproteinase families. Human genomics 4: 194-201. DOI 10.1186/1479-7364-4-3-194
11. Luedde T, Kaplowitz N, Schwabe RF (2014) Cell death and cell death responses in liver disease: mechanisms and clinical relevance. Gastroenterology 147: 765-783.e764. DOI 10.1053/j.gastro.2014.07.018
12. Schwabe RF, Luedde T (2018) Apoptosis and necroptosis in the liver: a matter of life and death. Nature reviews Gastroenterology & hepatology 15: 738-752. DOI 10.1038/s41575-018-0065-y
13. Stanger BZ, Leder P, Lee TH, Kim E, Seed B (1995) RIP: a novel protein containing a death domain that interacts with Fas/APO-1 (CD95) in yeast and causes cell death. Cell 81: 513-523. DOI 10.1016/0092-8674(95)90072-1

14. Hsu H, Huang J, Shu HB, Baichwal V, Goeddel DV (1996) TNF-dependent recruitment of the protein kinase RIP to the TNF receptor-1 signaling complex. Immunity 4: 387-396. DOI 10.1016/s1074-7613(00)80252-6
15. Chaudhary PM, Eby M, Jasmin A, Bookwalter A, Murray J, Hood L (1997) Death receptor 5, a new member of the TNFR family, and DR4 induce FADD-dependent apoptosis and activate the NF-kappaB pathway. Immunity 7: 821-830. DOI 10.1016/s1074-7613(00)80400-8
16. Farooq M, Filliol A, Simoes Eugénio M, Piquet-Pellorce C, Dion S, Raguenes-Nicol C, Jan A, Dimanche-Boitrel MT, Le Seyec J, Samson M (2019) Depletion of RIPK1 in hepatocytes exacerbates liver damage in fulminant viral hepatitis. Cell death & disease 10: 12. DOI 10.1038/s41419-018-1277-3
17. Filliol A, Piquet-Pellorce C, Le Seyec J, Farooq M, Genet V, Lucas-Clerc C, Bertin J, Gough PJ, Dimanche-Boitrel MT, Vandenabeele P, et al. (2016) RIPK1 protects from TNF-α-mediated liver damage during hepatitis. Cell death & disease 7: e2462. DOI 10.1038/cddis.2016.362
18. Brun P, Castagliuolo I, Di Leo V, Buda A, Pinzani M, Palù G, Martines D (2007) Increased intestinal permeability in obese mice: new evidence in the pathogenesis of nonalcoholic steatohepatitis. American journal of physiology Gastrointestinal and liver physiology 292: G518-525. DOI 10.1152/ajpgi.00024.2006
19. Ilan Y (2012) Leaky gut and the liver: a role for bacterial translocation in nonalcoholic steatohepatitis. World journal of gastroenterology 18: 2609-2618. DOI 10.3748/wjg.v18.i21.2609
20. Luther J, Garber JJ, Khalili H, Dave M, Bale SS, Jindal R, Motola DL, Luther S, Bohr S, Jeoung SW, et al. (2015) Hepatic Injury in Nonalcoholic Steatohepatitis Contributes to Altered Intestinal Permeability. Cellular and molecular gastroenterology and hepatology 1: 222-232. DOI 10.1016/j.jcmgh.2015.01.001
21. Miele L, Valenza V, La Torre G, Montalto M, Cammarota G, Ricci R, Mascianà R, Forgione A, Gabrieli ML, Perotti G, et al. (2009) Increased intestinal permeability and tight junction alterations in nonalcoholic fatty liver disease. Hepatology (Baltimore, Md) 49: 1877-1887. DOI 10.1002/hep.22848
22. Filliol A, Piquet-Pellorce C, Raguénès-Nicol C, Dion S, Farooq M, Lucas-Clerc C, Vandenabeele P, Bertrand MJM, Le Seyec J, Samson M (2017) RIPK1 protects hepatocytes from Kupffer cells-mediated TNF-induced apoptosis in mouse models of PAMP-induced hepatitis. Journal of hepatology 66: 1205-1213. DOI 10.1016/j.jhep.2017.01.005
23. Schneider AT, Gautheron J, Feoktistova M, Roderburg C, Loosen SH, Roy S, Benz F, Schemmer P, Büchler MW, Nachbur U, et al. (2017) RIPK1 Suppresses a TRAF2-Dependent Pathway to Liver Cancer. Cancer cell 31: 94-109. DOI 10.1016/j.ccell.2016.11.009
24. Van TM, Polykratis A, Straub BK, Kondylis V, Papadopoulou N, Pasparakis M (2017) Kinase-independent functions of RIPK1 regulate hepatocyte survival and liver carcinogenesis. The Journal of clinical investigation 127: 2662-2677. DOI 10.1172/jci92508

25. Majdi A, Aoudjehane L, Ratziu V, Islam T, Afonso MB, Conti F, Mestiri T, Lagouge M, Foufelle F, Ballenghien F, et al. (2020) Inhibition of receptor-interacting protein kinase 1 improves experimental non-alcoholic fatty liver disease. Journal of hepatology 72: 627-635. DOI 10.1016/j.jhep.2019.11.008
26. Tao L, Yi Y, Chen Y, Zhang H, Orning P, Lien E, Jie J, Zhang W, Xu Q, Li Y, et al. (2020) RIP1 kinase activity promotes steatohepatitis through mediating cell death and inflammation in macrophages. Cell death and differentiation. DOI 10.1038/s41418-020-00668-w
27. Matsuzawa N, Takamura T, Kurita S, Misu H, Ota T, Ando H, Yokoyama M, Honda M, Zen Y, Nakanuma Y, et al. (2007) Lipid-induced oxidative stress causes steatohepatitis in mice fed an atherogenic diet. Hepatology (Baltimore, Md) 46: 1392-1403. DOI 10.1002/hep.21874
28. Tiniakos DG, Vos MB, Brunt EM (2010) Nonalcoholic fatty liver disease: pathology and pathogenesis. Annual review of pathology 5: 145-171. DOI 10.1146/annurev-pathol-121808-102132
29. Brunt EM, Janney CG, Di Bisceglie AM, Neuschwander-Tetri BA, Bacon BR (1999) Nonalcoholic steatohepatitis: a proposal for grading and staging the histological lesions. The American journal of gastroenterology 94: 2467-2474. DOI 10.1111/j.1572-0241.1999.01377.x
30. Diana J, Beaudoin L, Gautron AS, Lehuen A (2011) NKT and tolerance. Methods in molecular biology (Clifton, NJ) 677: 193-206. DOI 10.1007/978-1-60761-869-0_14
31. Lisbonne M, L'Helgoualc'h A, Nauwelaers G, Turlin B, Lucas C, Herbelin A, Piquet-Pellorce C, Samson M (2011) Invariant natural killer T-cell-deficient mice display increased CCl_4 -induced hepatitis associated with CXCL1 over-expression and neutrophil infiltration. European journal of immunology 41: 1720-1732. DOI 10.1002/eji.201041006
32. Vasseur P, Dion S, Filliol A, Genet V, Lucas-Clerc C, Jean-Philippe G, Silvain C, Lecron JC, Piquet-Pellorce C, Samson M (2017) Endogenous IL-33 has no effect on the progression of fibrosis during experimental steatohepatitis. Oncotarget 8: 48563-48574. DOI 10.18632/oncotarget.18335
33. Liang S, Kisseleva T, Brenner DA (2016) The Role of NADPH Oxidases (NOXs) in Liver Fibrosis and the Activation of Myofibroblasts. Frontiers in physiology 7: 17. DOI 10.3389/fphys.2016.00017
34. Feldstein AE, Canbay A, Angulo P, Taniai M, Burgart LJ, Lindor KD, Gores GJ (2003) Hepatocyte apoptosis and fas expression are prominent features of human nonalcoholic steatohepatitis. Gastroenterology 125: 437-443. DOI 10.1016/s0016-5085(03)00907-7
35. Feldstein AE, Werneburg NW, Canbay A, Guicciardi ME, Bronk SF, Rydzewski R, Burgart LJ, Gores GJ (2004) Free fatty acids promote hepatic lipotoxicity by stimulating TNF-alpha expression via a lysosomal pathway. Hepatology (Baltimore, Md) 40: 185-194. DOI 10.1002/hep.20283

36. Idrissova L, Malhi H, Werneburg NW, LeBrasseur NK, Bronk SF, Fingas C, Tchkonia T, Pirtskhalava T, White TA, Stout MB, et al. (2015) TRAIL receptor deletion in mice suppresses the inflammation of nutrient excess. Journal of hepatology 62: 1156-1163. DOI 10.1016/j.jhep.2014.11.033
37. Filliol A, Farooq M, Piquet-Pellorce C, Genet V, Dimanche-Boitrel MT, Vandenabeele P, Bertrand MJM, Samson M, Le Seyec J (2017) RIPK1 protects hepatocytes from death in Fas-induced hepatitis. Scientific reports 7: 9205. DOI 10.1038/s41598-017-09789-8
38. Pasparakis M, Vandenabeele P (2015) Necroptosis and its role in inflammation. Nature 517: 311-320. DOI 10.1038/nature14191
39. Degterev A, Hitomi J, Germscheid M, Ch'en IL, Korkina O, Teng X, Abbott D, Cuny GD, Yuan C, Wagner G, et al. (2008) Identification of RIP1 kinase as a specific cellular target of necrostatins. Nature chemical biology 4: 313-321. DOI 10.1038/nchembio.83
40. Afonso MB, Rodrigues PM, Carvalho T, Caridade M, Borralho P, Cortez-Pinto H, Castro RE, Rodrigues CM (2015) Necroptosis is a key pathogenic event in human and experimental murine models of non-alcoholic steatohepatitis. Clinical science (London, England : 1979) 129: 721-739. DOI 10.1042/cs20140732
41. von Montfort C, Matias N, Fernandez A, Fucho R, Conde de la Rosa L, Martinez-Chantar ML, Mato JM, Machida K, Tsukamoto H, Murphy MP, et al. (2012) Mitochondrial GSH determines the toxic or therapeutic potential of superoxide scavenging in steatohepatitis. Journal of hepatology 57: 852-859. DOI 10.1016/j.jhep.2012.05.024
42. Takahashi N, Duprez L, Grootjans S, Cauwels A, Nerinckx W, DuHadaway JB, Goossens V, Roelandt R, Van Hauwermeiren F, Libert C, et al. (2012) Necrostatin-1 analogues: critical issues on the specificity, activity and in vivo use in experimental disease models. Cell death & disease 3: e437. DOI 10.1038/cddis.2012.176
43. Schuster S, Cabrera D, Arrese M, Feldstein AE (2018) Triggering and resolution of inflammation in NASH. Nature reviews Gastroenterology & hepatology 15: 349-364. DOI 10.1038/s41575-018-0009-6
44. Hua J, Ma X, Webb T, Potter JJ, Oelke M, Li Z (2010) Dietary fatty acids modulate antigen presentation to hepatic NKT cells in nonalcoholic fatty liver disease. Journal of lipid research 51: 1696-1703. DOI 10.1194/jlr.M003004
45. Li Z, Soloski MJ, Diehl AM (2005) Dietary factors alter hepatic innate immune system in mice with nonalcoholic fatty liver disease. Hepatology (Baltimore, Md) 42: 880-885. DOI 10.1002/hep.20826
46. Tang T, Sui Y, Lian M, Li Z, Hua J (2013) Pro-inflammatory activated Kupffer cells by lipids induce hepatic NKT cells deficiency through activation-induced cell death. PloS one 8: e81949. DOI 10.1371/journal.pone.0081949
47. Jarrar MH, Baranova A, Collantes R, Ranard B, Stepanova M, Bennett C, Fang Y, Elariny H, Goodman Z, Chandhoke V, et al. (2008) Adipokines and cytokines in non-alcoholic fatty liver disease. Alimentary pharmacology & therapeutics 27: 412-421. DOI 10.1111/j.1365-2036.2007.03586.x

48. Cuchet-Lourenço D, Eletto D, Wu C, Plagnol V, Papapietro O, Curtis J, Ceron-Gutierrez L, Bacon CM, Hackett S, Alsaleem B, et al. (2018) Biallelic RIPK1 mutations in humans cause severe immunodeficiency, arthritis, and intestinal inflammation. Science (New York, NY) 361: 810-813. DOI 10.1126/science.aar2641
49. Bataller R, Brenner DA (2005) Liver fibrosis. The Journal of clinical investigation 115: 209-218. DOI 10.1172/jci24282
50. Gäbele E, Brenner DA, Rippe RA (2003) Liver fibrosis: signals leading to the amplification of the fibrogenic hepatic stellate cell. Frontiers in bioscience : a journal and virtual library 8: d69-77. DOI 10.2741/887
51. Duarte S, Baber J, Fujii T, Coito AJ (2015) Matrix metalloproteinases in liver injury, repair and fibrosis. Matrix biology : journal of the International Society for Matrix Biology 44-46: 147-156. DOI 10.1016/j.matbio.2015.01.004

Figure legends

Fig. 1 Diet-induced NASH led to increased transcript rates of death factor/receptor pairs and RIPK1 in mouse liver

C57Bl6/J male mice received either a SD (0) (empty black circles) or a HFHCD during 12 weeks (solid black circles). Relative levels of *Tnf*, *Tnfr1*, *Tnfr2*, *Fas-l*, *Fas*, *Trail*, *Dr5* and *Ripk1* transcripts quantified in liver tissue from all animals and individually represented by a symbol.

Fig. 2 Development of diet-induced NASH clinical signs in *Ripk1*$^{fl/fl}$ and *Ripk1*$^{LPC\text{-}KO}$ mice

Ripk1$^{fl/fl}$ and *Ripk1*$^{LPC\text{-}KO}$ C57Bl6/J male mice received either a SD (0) or a HFHCD during 3, 5 or 12 weeks. (A) Evolution of the body weight (left panel) and of the liver to body weight ratio (right panel) followed over time. (B) Levels of serum alanine aminotransferase. (C) Representative pictures of liver tissue sections analysed by Oil-Red O staining (left panel; black bars represent 100 µm) with specific-signal quantification (right panel). (D) Representative pictures of liver tissue sections stained by H&E (black arrows show immune cell infiltrates; black bars represent 100 µm). (E) NAS score (dark grey, light grey and white bars respectively represent the evaluation of hepatocyte ballooning, inflammation and steatosis). For all graphs, each empty and solid black circles respectively represent *Ripk1*$^{fl/fl}$ individuals under SD or HFHCD, while empty and solid grey squares respectively represent *Ripk1*$^{LPC\text{-}KO}$ individuals under SD or HFHCD.

Fig. 3 Modulation of cytokine expression during diet-induced NASH in *Ripk1*$^{fl/fl}$ and *Ripk1*$^{LPC\text{-}KO}$ mice

Ripk1$^{fl/fl}$ and *Ripk1*$^{LPC\text{-}KO}$ C57Bl6/J male mice received either a SD (0) or a HFHCD during 3, 5 or 12 weeks. (A) Relative levels of *Tnf*, *Il6* and *Ccl2* transcripts quantified in liver tissue. (B) Levels of plasma TNF, IL6, CCL2, IL27 and IFNβ. See the Material and Methods section for consideration of detection limits. For all graphs, each empty and solid black circles respectively represent *Ripk1*$^{fl/fl}$ individuals under SD or HFHCD, while empty and solid grey squares respectively represent *Ripk1*$^{LPC\text{-}KO}$ individuals under SD or HFHCD.

Fig. 4 Analysis of hepatic immune infiltrates in *Ripk1*$^{fl/fl}$ and *Ripk1*$^{LPC\text{-}KO}$ mice with diet induced NASH

Ripk1$^{fl/fl}$ and *Ripk1*$^{LPC\text{-}KO}$ C57Bl6/J male mice received either a SD (0) or a HFHCD during 3, 5 or 12 weeks. Numbers of total immune cells, CD4+ T cells (LT4), CD8+ T cells (LT8), regulatory T cells (LTreg), Natural Killer (NK) cells, Natural Killer T (NKT) cells, B lymphocytes (LB), macrophages and neutrophils in the different experimental conditions. For all graphs, each empty and solid black circles respectively represent *Ripk1*$^{fl/fl}$ individuals under SD or HFHCD, while empty and solid grey squares respectively represent *Ripk1*$^{LPC\text{-}KO}$ individuals under SD or HFHCD.

Fig. 5 Fibrosis-related parameters in *Ripk1*$^{fl/fl}$ and *Ripk1*$^{LPC-KO}$ mice with diet-induced NASH

Ripk1$^{fl/fl}$ and *Ripk1*$^{LPC-KO}$ C57Bl6/J male mice received either a SD (0) or a HFHCD during 3, 5 or 12 weeks. (A) Representative pictures of liver tissue sections with Sirius Red staining (left panel; black bars represent 250 µm) and quantification of fibrosis as determined by the percentage of Sirius Red positive area (right panel). (B) hepatic mRNA expression levels of *Tgfb1*, *Col1a1*, *Tgfbi*, *Mmp2*, *Timp1*, *Timp2* and *Nox2* genes. For all graphs, each empty and solid black circles respectively represent *Ripk1*$^{fl/fl}$ individuals under SD or HFHCD, while empty and solid grey squares respectively represent *Ripk1*$^{LPC-KO}$ individuals under SD or HFHCD.

Figure 1

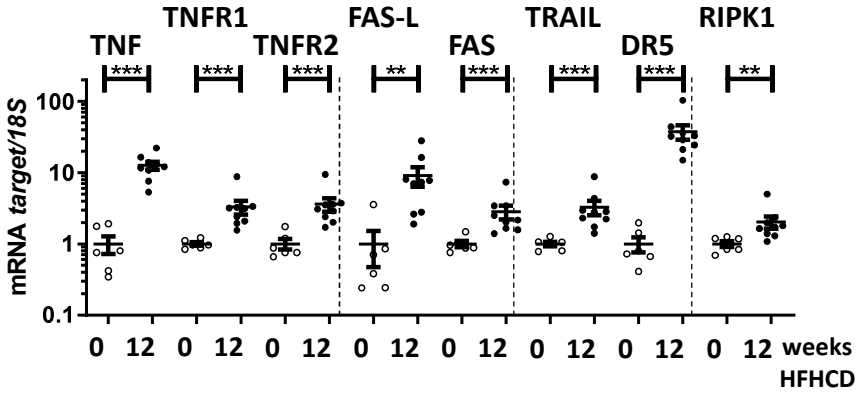

Figure 2

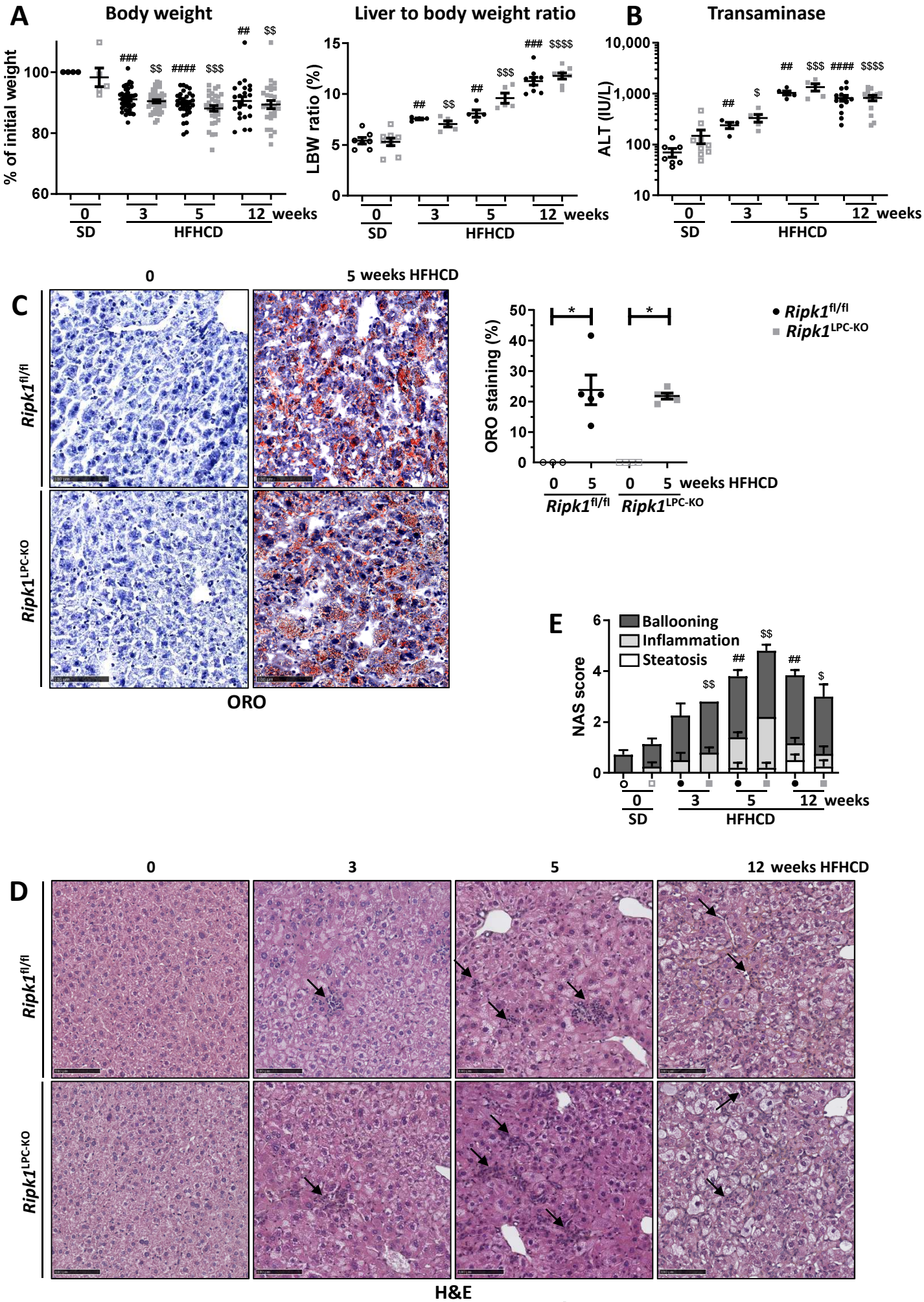

Figure 3

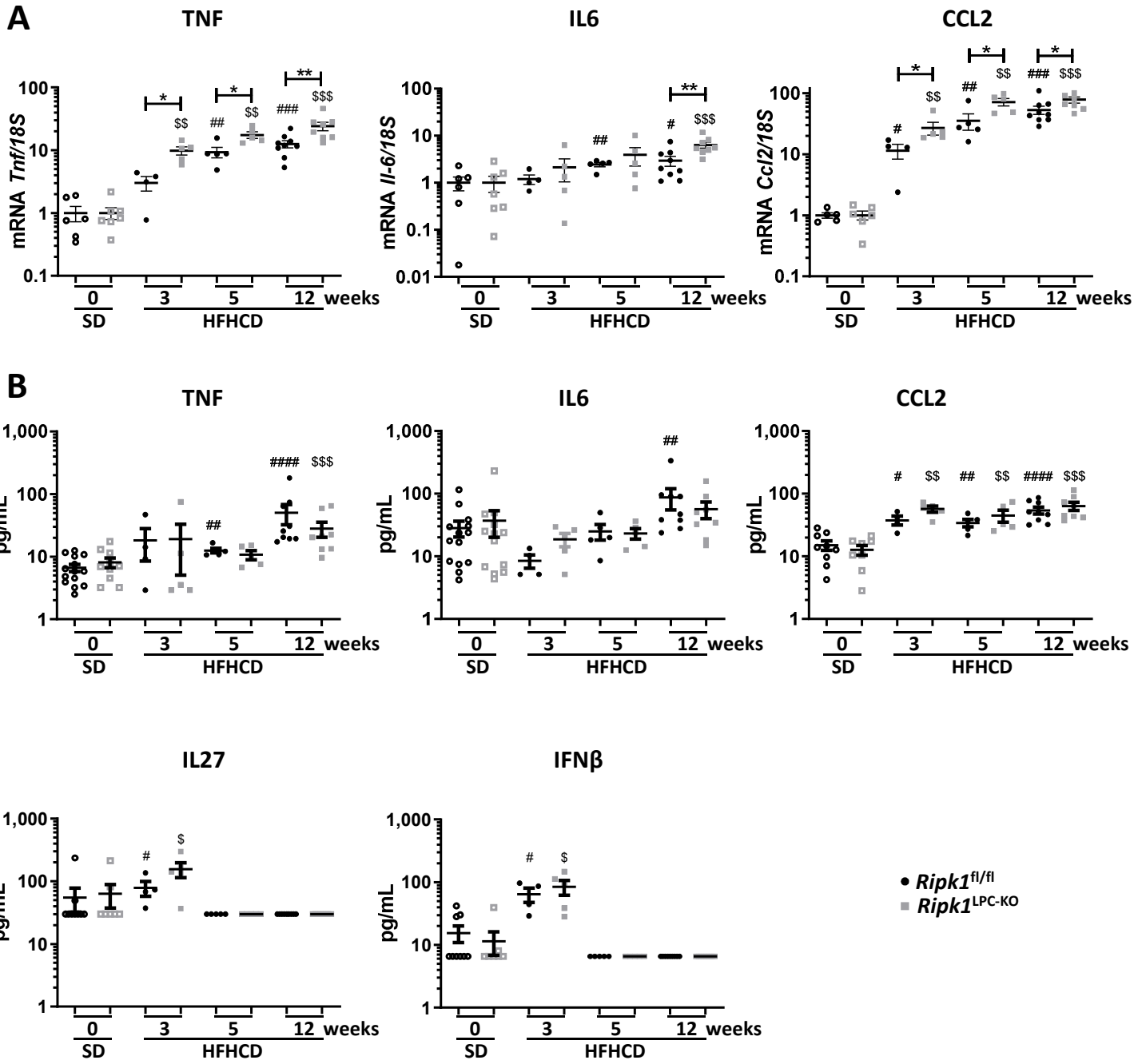

Figure 4

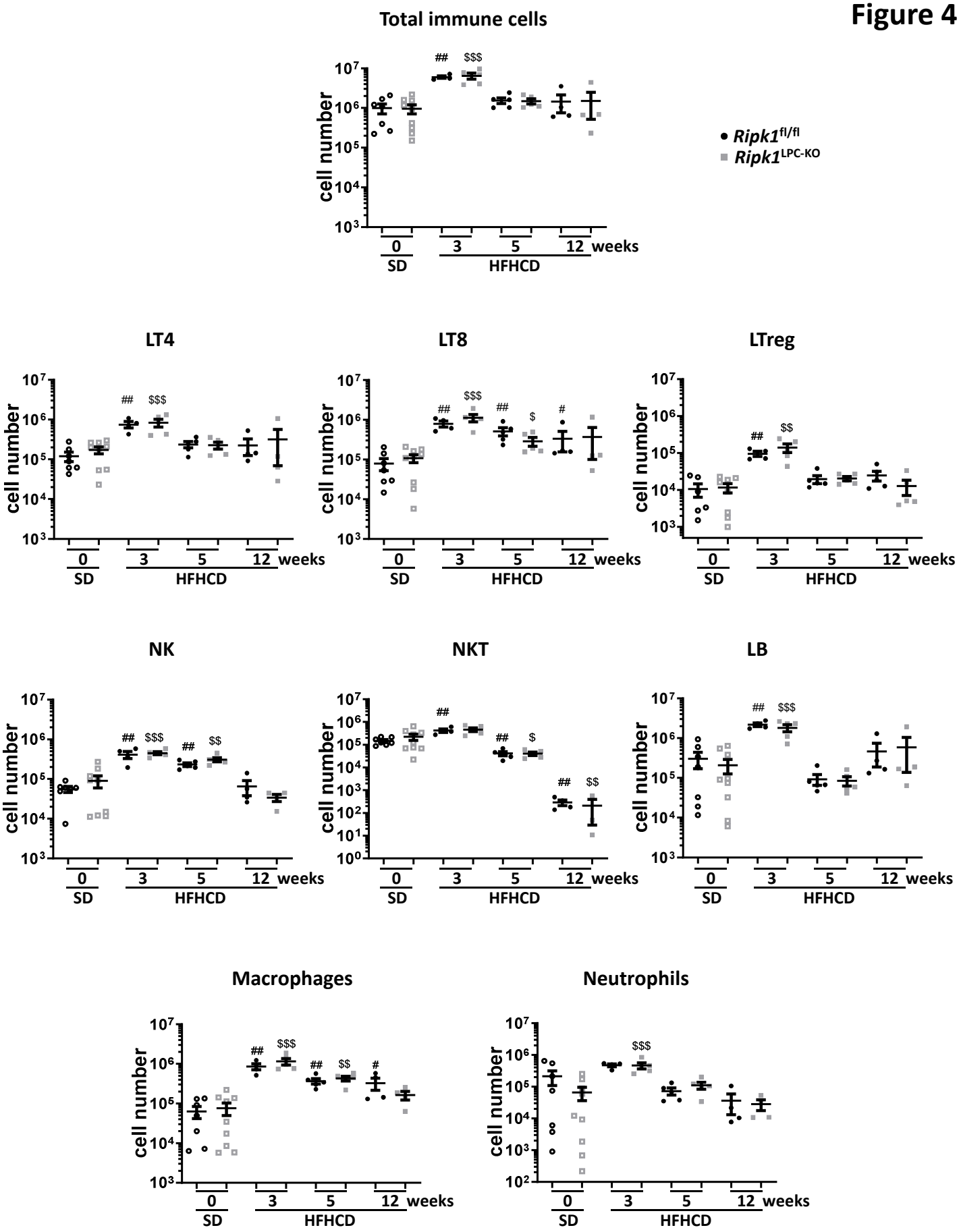

Figure 5

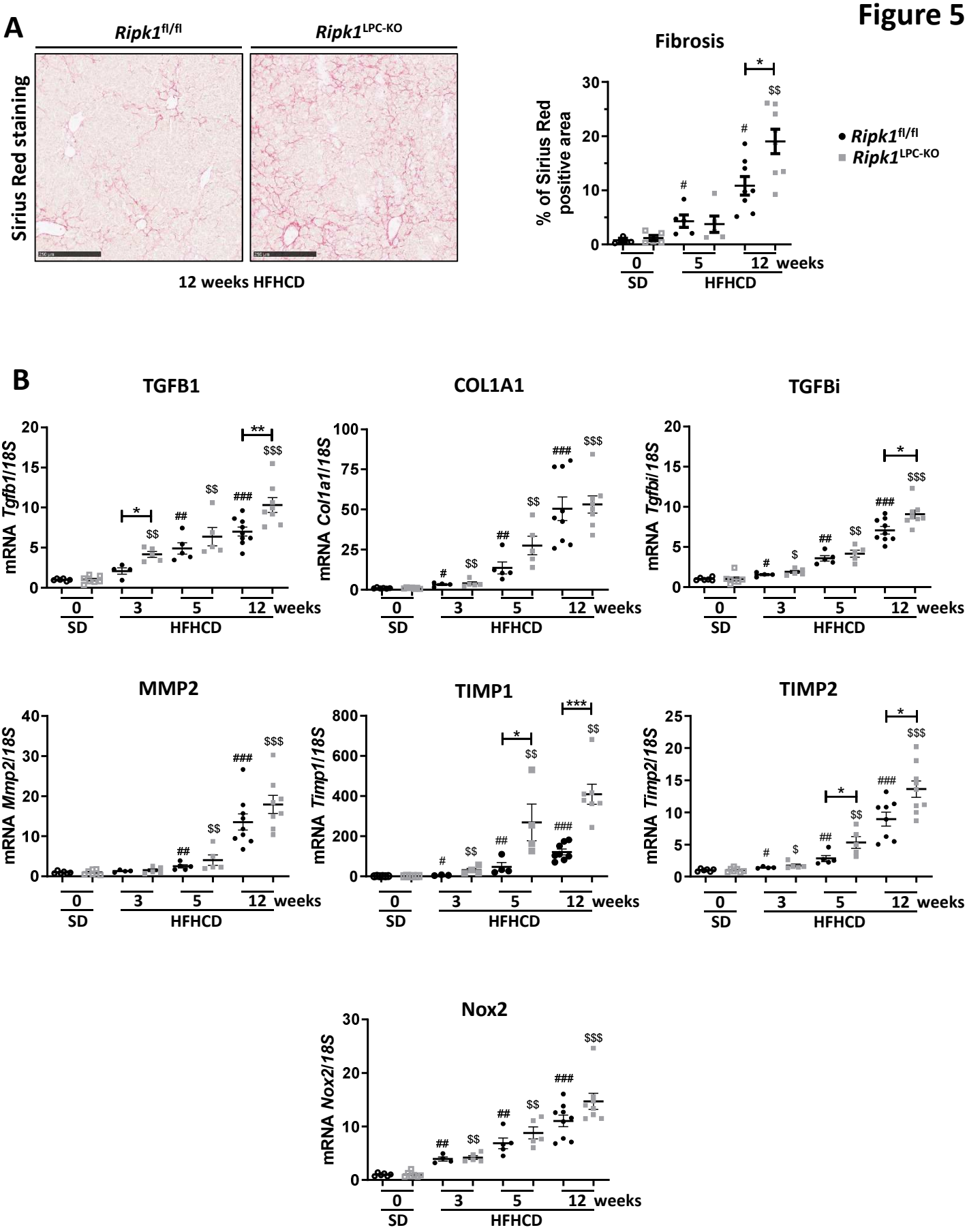

Table S1 Sequences of primers used for qPCR

Gene	Forward primer (5'-3')	Reverse primer (5'-3')
Rn18s	TTGGCAAATGCTTTCGCTC	CGCCGCTAGAGGTGAAATTC
Tnf	TAGCTCCCAGAAAAGCAAGC	TTTTCTGGAGGGAGATGTGG
Il6	CCGGAGAGGAGACTTCACAG	CAGAATTGCCATTGCACAAC
Timp1	TTCCAGTAAGGCCTGTAGC	TTATGACCAGGTCCGAGTT
Timp2	CTGGGACACGCTTAGCATCA	GACAGCGAGTGATCTTGCAC
Ccl2	TCCCAATGAGTAGGCTGGAG	TCTGGACCCATTCCTTCTTG
Nox2	AGTGCGTGTTGCTCGACAA	GCGGTGTGCAGTGCTATCAT
Col1a1	GCTCCTGCTCCTCTTAGGG	GCAGAAAGCACAGCACTCG
Mmp2	ATGGTAAACAAGGCTTCATG	TTGAGAAGGATGGCAAGTAT
Mmp8	TACAGGGAACCCAGCACCTA	GGGGTTGTCTGAAGGTCCATAG
Mmp9	CATTCGCGTGGATAAGGAGT	TCACACGCCAGAAGAATTTG
Mmp13	ACACTGGCAAAAGCCATTTC	TTTTGGGATGCTTAGGGTTG
Mmp14	GCCCTCTGTCCCAGATAAGC	ACCATCGCTCCTTGAAGACA
Mmp19	GTGTGGACTGTAACAGATTCAGG	CCTTGAAGAAATGAGTCCGTCGT
Tgfb1	CACCATCCATGACATGAACC	CAGAAGTTGGCATGGTAGCC

Table S2 List of fluorochrome-conjugated antibodies

Target	Fluorescent dye	Clone	Reference
CD3	APC	145.2.C11	eBio 17-0031-81
CD4	BV510	RM4-5	BD 561099
CD8	APC- Cy7	53-6-7	BD 557654
CD19	BV786	ID3	BD 563333
TCR	BV605	H57-597	BD 562840
FoxP3	PE	150D/E4	eBio 12-4774-42
NK1.1	PEeFluor	PK136	eBio 61-5941-80
CD11b	PE-Cy7	M1/70	BD 552850
GR1	Efluor 450	RB6-8C5	eBio 48-5931-82

All antibodies were purchased from either BD Pharmingen™ or eBioscience Thermo Fisher Scientific.

Figure 1S

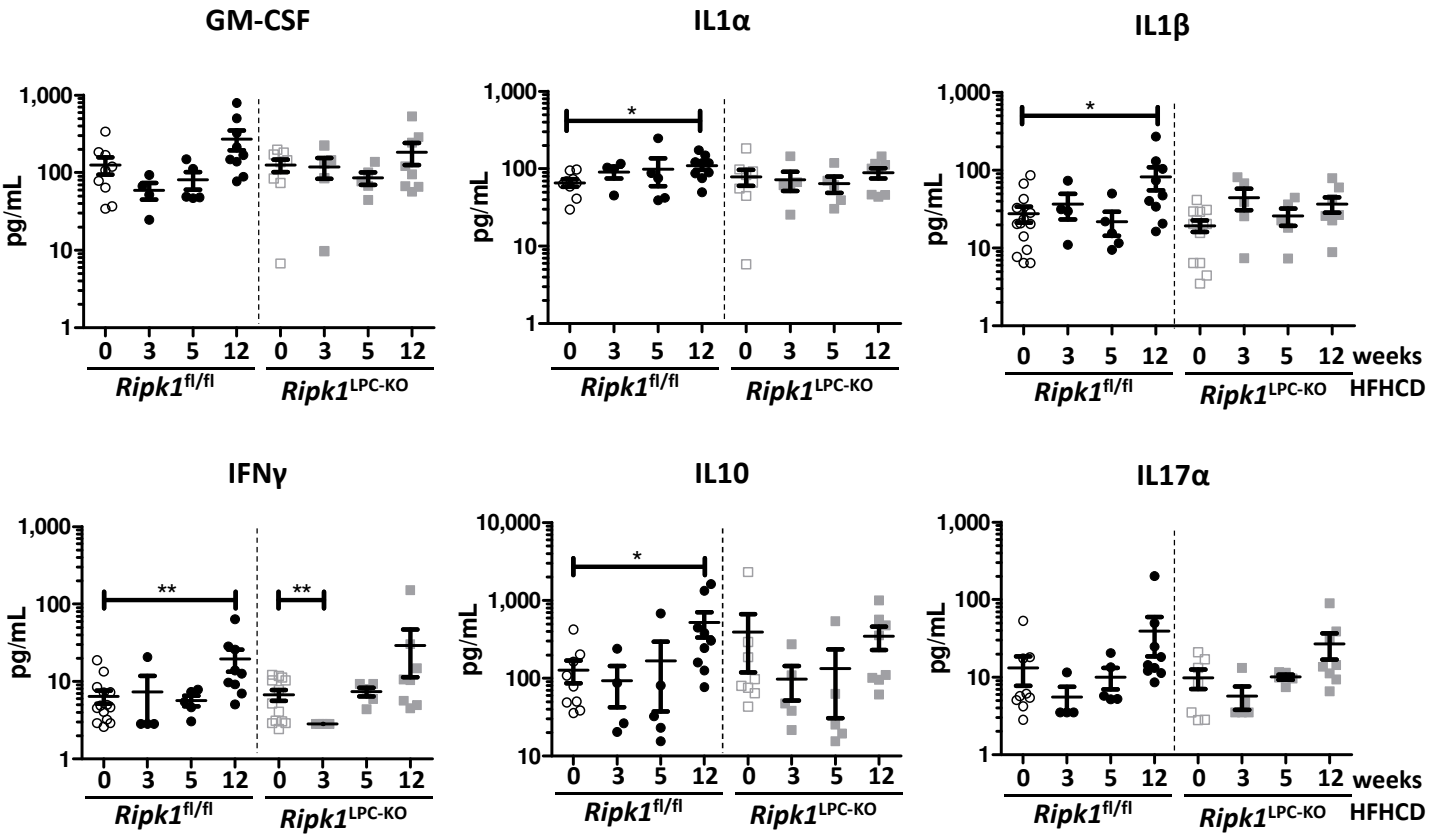

Fig. 1S Plasma concentrations of cytokines

Levels of plasma GM-CSF, IL1α, IL1β, IFNγ, IL10 and IL17α. Plasma concentrations of IL23 and IL12p70 are not shown because mostly below the detection threshold. See the Material and Methods section for consideration of detection limits. For all graphs, each empty and solid black circles respectively represent *Ripk1*$^{fl/fl}$ individuals under SD or HFHCD, while empty and solid grey squares respectively represent *Ripk1*$^{LPC\text{-}KO}$ individuals under SD or HFHCD.

Figure 2S

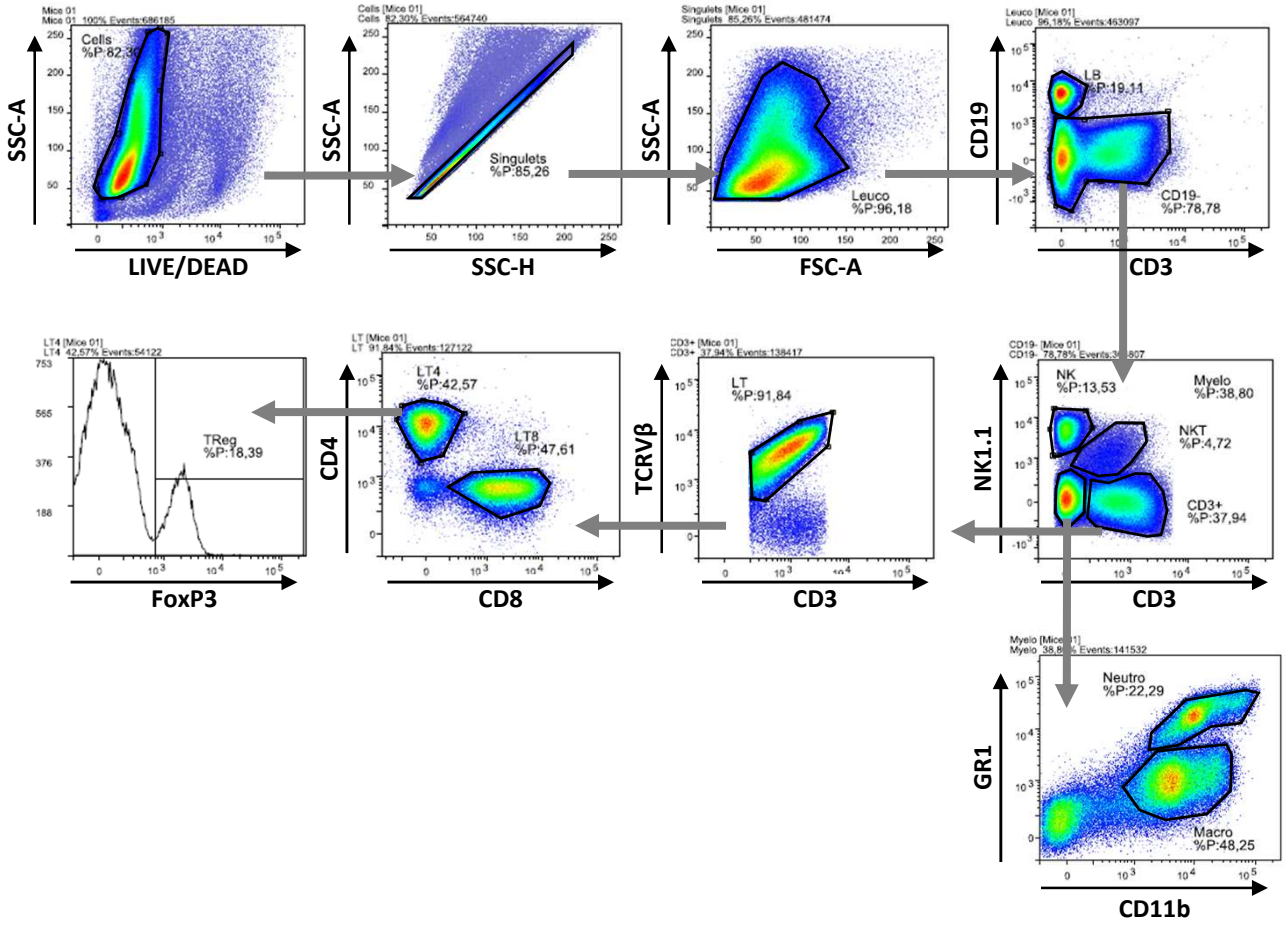

Fig. 2S Gating strategy used to identify the different populations of hepatic immune cells
Lymphocytes B (CD19+/CD3-), lymphocytes T-CD8+ (CD19-/CD3+/TCRVβ+/NK1.1-/CD8+), lymphocytes T-CD4+ (CD19-/CD3+/TCRVβ+/NK1.1-/CD4+), regulatory T cells (CD19-/CD3+/TCRVβ+/NK1.1-/CD4+/FoxP3+), NKT cells (CD19-/CD3+/NK1.1+), NK cells (CD19-/CD3-/NK1.1+), neutrophils (CD19-/CD3-/NK1.1-/GR1+/CD11b+) and macrophages (CD19-/CD3-/NK1.1-/GR1+/-/CD11b+) were first gated for singlets and on a viability marker (black arrows define x and y axes; thick grey arrows show the identification process of the immune cell populations).

Figure 3S

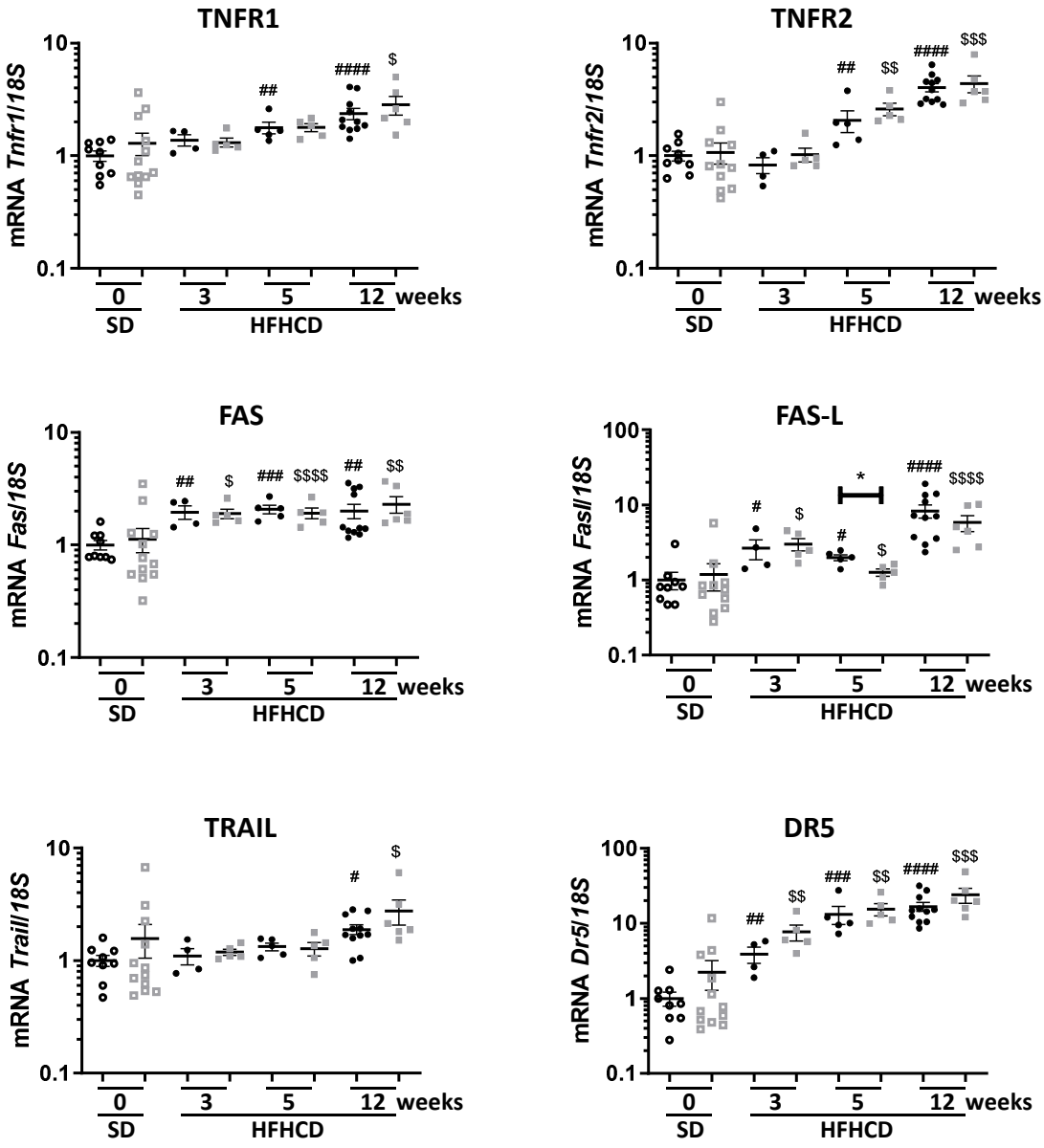

Fig. 3S Relative quantification of hepatic mRNA transcripts
Ripk1$^{fl/fl}$ and *Ripk1*$^{LPC\text{-}KO}$ C57Bl6/J male mice received either a SD (0) or a HFHCD during 3, 5 or 12 weeks. Relative levels of *Tnfr1*, *Tnfr2*, *Fas*, *Fasl*, *Trail* and *Dr5* transcripts quantified in liver tissue. For all graphs, each empty and solid black circles respectively represent *Ripk1*$^{fl/fl}$ individuals under SD or HFHCD, while empty and solid grey squares respectively represent *Ripk1*$^{LPC\text{-}KO}$ individuals under SD or HFHCD.